American Journal of Physical Chemistry
2025, Vol. 14, No. 3, pp. 77-90
https://doi.org/10.11648/j.ajpc.20251403.13

Research Article

Calculation and Analysis of the Thermophysical Properties of Air-Aerosols Mixtures

Yaguibou Wepari Charles[1, *], Pafadnam Ibrahim[2], Banouga Adjigkiga[3], Yann Cressault[4], Kagone Abdoul Karim[3], Kohio Niessan[5], Koalaga Zacharie[3]

[1]Dori University Center, Thomas Sankara University, Ouagadougou, Burkina Faso
[2]Science and Technology, Thomas Sankara University, Ouagadougou, Burkina Faso
[3]Materials and Environment Laboratory, Joseph Ki-Zerbo University, Ouagadougou, Burkina Faso
[4]Plasma and Energy Conversion Laboratory, UPS, INPT, Toulouse University, Toulouse, France
[5]Materials and Environment Laboratory, Superior Normal School, Koudougou, Burkina Faso

Abstract

Electrical equipment, such as circuit breakers, often encounters operational issues, such as short-circuit failures. These malfunctions can be attributed to the deposition of aerosols containing aluminium oxide (Al_2O_3), calcium oxide (CaO), ferric oxide (Fe_2O_3), and silica (SiO_2) on the devices. Previous studies have examined the influence of dust particles, such as silica, on the performances of circuit breakers. Silica significantly modifies molar fractions, leading to the formation of solid and liquid phases of SiO_2 that condense on the surfaces of the gas generator. This results in changes to the dynamic viscosity of the arc, its motion and speed. However, these recent studies did not consider the combined effects of various species, including Fe_2O_3, CaO, Al_2O_3, and CO, which can be present in dust deposits depending on regional environmental conditions. To enhance the protection of circuit breakers from dust, this study investigates the effect of aerosols on the transport coefficients of air plasma in local thermodynamic equilibrium (LTE), for atmospheric pressure and temperatures ranging from 2,000 K to 30,000 K. Transport coefficients are calculated using the Chapman-Enskog method. The findings reveal alterations in the transport properties of the electric arc plasma during the circuit-breaking process. A reduction in thermal conductivity, and dynamic viscosity with increasing temperature is observed. However, thermal conductivity increases at 4,000 K, respectively, and both the mass density and electrical conductivity of the plasma increase with temperature. Consequently, the presence of these aerosols within the circuit breaker during the cutoff phase adversely affects its performance, potentially leading to leakage currents post-operation or even to fire hazards in cases of unsuccessful circuit interruption.

Keywords

Electrical, Thermal, Conductivity, Viscosity, Plasma, Circuit Breaker

[*]Corresponding author: weparicharles@gmail.com (Yaguibou Wepari Charles)

Received: 20 July 2025; **Accepted:** 19 August 2025; **Published:** 19 September 2025

1. Introduction

Dust is an environmental factor that can accelerate the ageing and malfunction of electrical equipment. The West African region, located within the intertropical zone, extends from 4 ℕ to the southern edge of the Sahara (~20 ℕ) and from 18 ℚ to 20 ℰ (eastern border of Lake Chad) [1]. This region is a significant source of desert aerosols, including dust particles, sand, pollen, volcanic ash, and sea spray. The transport of these particles through West Africa is largely influenced by regional atmospheric dynamics, particularly the Harmattan and monsoon winds [1-5].

The chemical composition of aerosols in West Africa varies depending on soil characteristics. They are typically composed of aluminium Al_2O_3, calcium CaO, ferric Fe_2O_3, and silica SiO_2 [6-13]. The most abundant chemical compounds in aerosols are silicon, calcium, ferric, and aluminium oxides. Carbon oxide species originate from biomass fires and fossilfuel production. Furthermore, silica represents up to 60% of the total mass. After silica, the most abundant oxides are aluminium oxides (Al_2O_3) and ferric oxides (Fe_2O_3) [10, 11]. The composition and concentration of the chemical compounds in aerosols vary depending on the area. The proportions of the mass considered in this work are related to desert sandstorms, to the composition of the soil in the region and to human activities. SiO_2 is the dominant species. In Ouagadougou, the red colour of the dust indicates the presence of Fe_2O_3 in a higher proportion than CaO or Al_2O_3 which nevertheless have non-negligible concentrations. The literature does not provide any work presenting a clear composition of aerosols. Some works usually focus on specific chemical species (and their mass fractions) directly dependent on the region studied [1, 3, 9-11]. Therefore, desert aerosols combine with anthropogenic pollutants, such as hydrocarbons [14, 15]. This heterogeneous mixture then accumulates in electrical equipment, including circuit breakers. Through air vents, the mixture enters circuit breakers and is deposited on the electrodes and inside the break chamber [16, 17]. Figures 1 to 2 show dust episodes and accumulation on circuit breakers. Recent studies have demonstrated the impact of dust particles, such as silica, on circuit breaker performance [16, 17]. Silica significantly modifies the molar fractions, forming the solid and liquid phases of SiO_2 that condense on the surfaces of the gas generator. This process changes the dynamic viscosity of the arc, its motion and speed [16, 17]. Aerosols can degrade electrical circuits and circuit breaker components. However, previous studies did not examine the combined effects of various species, including Fe_2O_3, CaO, Al_2O_3, and CO, which can be present in dust deposits depending on regional conditions. This study aims to investigate the effects of aerosols on the transport coefficients of plasma in the West African region.

The remainder of this paper is organised as follows: Section 2 describes the methods for computing transport coefficients; Section 3 discusses the effects of aerosols on these properties; and Section 4 presents the conclusions.

Figure 1. *Dust storm in Ouagadougou in 2024 (https://netafrique.net).*

Figure 2. *Dust deposition on circuit breakers [16].*

2. Methods and Materials

A circuit breaker may be required to operate in a polluted environment for a long time. From a review of the literature, aerosols are mainly composed of silica, ferric oxides, aluminium oxides, calcium oxides, and carbon monoxide. In this work, we assume that 1 g of aerosol consists of 50% SiO_2, 20% Fe_2O_3, 10% Al_2O_3, 5% CO, and 15% CaO in mass proportions. The percentages were determined based on the estimated proportions of the studies, as there are no studies that provide the exact proportions of aerosols in this region. This work is entirely theoretical because the experimental setup and associated diagnostic equipment are very expensive.

In this study, the plasma is supposed to be in LTE for temperatures between 2,000 and 30,000 K, assuming only gaseous phases. All the results of the transport coefficients are presented at atmospheric pressure (1 atm).

2.1. Transport Coefficients

Based on Sonine polynomial expansions, we used the well-known Chapman-Enskog method to solve the Boltzmann equation and determine the transport coefficients [18].

2.1.1. Electrical Conductivity ($\Omega^{-1}m^{-1}$)

Devoto developed a third-order approximation to calculate the electrical conductivity of a partially ionised gas [19], written as:

$$\sigma = \frac{3}{2} e^2 n_1^2 \left[\frac{2\pi}{m_1 k_b T}\right]^{1/2} \frac{\begin{vmatrix} q^{11} & q^{12} \\ q^{21} & q^{22} \end{vmatrix}}{\begin{vmatrix} q^{00} & q^{01} & q^{02} \\ q^{10} & q^{11} & q^{12} \\ q^{20} & q^{21} & q^{22} \end{vmatrix}} \quad (1)$$

where k_b is the Boltzmann constant, and n_1 and m_1 are the density of the population number (m^{-3}) and the mass (kg) of the electrons, respectively. q^{ij} are functions depending on the population number densities of the particles and average effective collision cross-sections.

2.1.2. Thermal Conductivity ($W.m^{-1}.K^{-1}$)

The total thermal conductivity λ_{tot} of the plasma was calculated by adding the four terms described below:

$$\lambda_{tot} = \lambda_{tr}^{h} + \lambda_{tr}^{e} + \lambda_{int} + \lambda_{reac} \quad (2)$$

λ_{tr}^{h} is the translational contribution of heavy particles obtained using a second-order approximation:

$$\lambda_{tr}^{h} = 4 \frac{\begin{vmatrix} L_{11} & \cdots & L_{1v} & x_1 \\ \cdots & L_{ii} & \cdots & \cdots \\ L_{v1} & \cdots & L_{vv} & x_v \\ x_1 & \cdots & x_v & 0 \end{vmatrix}}{\begin{vmatrix} L_{11} & \cdots & L_{1v} \\ \cdots & \cdots & \cdots \\ L_{v1} & \cdots & L_{vv} \end{vmatrix}} \quad (3)$$

The coefficients L_{ij} are given by Muckenfuss [20].

λ_{tr}^{e} is the translational contribution of electrons expressed in the third-order approximation by Devoto [19, 21]:

$$\lambda_{tr}^{e} = \frac{75}{8} n_1^2 k_b \sqrt{\frac{2\pi k_b T}{m_1}} \frac{q^{22}}{q^{11}q^{22} - \left(q^{12}\right)^2} \quad (4)$$

where the functions q^{ij} are the same as those used for the electrical conductivity.

λ_{int} is the internal conductivity caused by the effect of the internal degrees of freedom and was calculated considering the Eucken correct [22, 23] as follows:

$$\lambda_{int} = \sum_{i=1}^{N} \frac{\left(\lambda_{int}\right)_i}{\sum_{\substack{j=1 \\ j\neq i}}^{N} \frac{D_{ii}(1)x_j}{D_{ij}(1)x_i}} \quad (5)$$

with $\left(\lambda_{int}\right)_i$ the internal conductivity of the chemical species i, and $D_{ij}(1)$ the binary diffusion coefficients deduced using the first-order approximation.

λ_{reac} is the reactive thermal conductivity which describes the transport of chemical enthalpy through temperature gradients. This coefficient was calculated using the general theory of diffusion fluxes by assuming a compact form under the hypothesis of local chemical equilibrium along the temperature gradient. For a system of υ independent chemical reactions (dissociation, ionisation) and μ chemical species, we used the Butler and Brokaw equation [21, 24-26]:

$$\lambda_{reac} = -\frac{1}{RT^2} \frac{\begin{vmatrix} A_{11} & \cdots & A_{1\vartheta} & \Delta H_1 \\ \vdots & \ddots & \vdots & \vdots \\ A_{\vartheta 1} & \cdots & A_{\vartheta\vartheta} & \Delta H_\vartheta \\ \Delta H_1 & \cdots & \Delta H_\vartheta & 0 \end{vmatrix}}{\begin{vmatrix} A_{11} & \cdots & A_{1\vartheta} \\ \vdots & \ddots & \vdots \\ A_{\vartheta 1} & \cdots & A_{\vartheta\vartheta} \end{vmatrix}} \quad (6)$$

with

$$A_{ij} = \sum_{k=1}^{\vartheta-1} \sum_{l=k+1}^{\vartheta} \frac{RT}{PD_{kl}(1)} x_k x_l \left(\frac{a_{ik}}{x_k} - \frac{a_{il}}{x_l}\right)\left(\frac{a_{jk}}{x_k} - \frac{a_{jl}}{x_l}\right) \quad (7)$$

$$D_{ij} = \frac{2{,}628.10^{-2}}{P} \frac{T^{3/2}}{\overline{\Omega}_{ij}^{(1,1)}} \left(\frac{M_i + M_j}{2M_i M_j}\right)^{1/2} \quad (8)$$

where ΔH_i is the enthalpy variation during the i^{th} reaction [21, 26].

2.1.3. Viscosity ($kg.m^{-1}s^{-1}$)

The viscosity can be attributed to heavy chemical species due to the low mass of electrons. The viscosity was thus calculated as follows [26, 27]:

$$\eta = -\frac{\begin{vmatrix} H_{11} & \cdots & H_{1\mu} & x_1 \\ \vdots & \ddots & \vdots & \vdots \\ H_{\mu 1} & \cdots & H_{\mu\mu} & x_\mu \\ x_1 & \cdots & x_\mu & 0 \end{vmatrix}}{\begin{vmatrix} H_{11} & \cdots & H_{1\mu} \\ \vdots & \ddots & \vdots \\ H_{\mu 1} & \cdots & H_{\mu\mu} \end{vmatrix}} \quad (9)$$

where

$$H_{ii} = \frac{x_i^2}{\eta_i} \sum_{\substack{k=1 \\ k=i}}^{\nu} \left(\frac{2x_i x_k}{\eta_{ik}} \frac{M_i M_k}{\left(M_i + M_k\right)^2} \left[\frac{5\overline{\Omega}_{ik}^{(1,1)}}{3\overline{\Omega}_{ik}^{(2,2)}} + \frac{M_k}{M_i} \right] \right) \quad (10)$$

$$H_{ij} = -\frac{2x_i x_j}{\eta_{ij}} \frac{M_i M_j}{\left(M_i + M_j\right)^2} \left[\frac{5\overline{\Omega}_{ij}^{(1,1)}}{3\overline{\Omega}_{ij}^{(2,2)}} - 1 \right] \quad (11)$$

$$n_i = 2.6693 * 10^{-6} \frac{\sqrt{M_i T}}{\overline{\Omega}_{ii}^{(2,2)}} \quad (12)$$

$$n_{ij} = 2.6693 * 10^{-6} \frac{\sqrt{2\left(\frac{M_i M_j}{M_i + M_j}\right)}}{\overline{\Omega}_{ij}^{(2,2)}} \quad (13)$$

with μ the total number of reactions considered, and $\overline{\Omega}_{ij}^{(l,s)}$ the collision integrals for each collision between two particles i and j (defined in the next section).

2.2. Collision Integrals

In thermal plasmas, the transport coefficients are calculated based on a specific method for solving the Boltzmann equation, known as the Chapman-Enskog method, which was presented in exhaustive detail by Hirschfelder [28]. According to this method, transport properties are obtained by computing collision integrals. These functions characterise an interaction between two particles i and j [28] and are expressed as follows:

$$\overline{\Omega}_{ij}^{(l,s)} = \left(\frac{k_b T}{2\pi\mu_{ij}} \right)^{1/2} \int_0^\infty \exp\left(-\gamma_{ij}^2\right) \gamma_{ij}^{2s+3} Q_{ij}^{(l)}\left(\varepsilon_r\right) d\gamma_{ij} \quad (14)$$

where $\gamma_{ij} = \left(\varepsilon_r / k_b T\right)^{1/2}$ is the relative velocity, μ_{ij} is the reduced mass and ε_r is the kinetic energy.

The term $Q_{ij}^{(l)}\left(\varepsilon_r\right)$ is the momentum transport cross-section which depends on the differential cross-sections, and consequently, on the interaction potentials [19, 21, 23]. calculation of the collision integrals was made by considering four types of interactions: neutral-neutral interactions, neutral-ion interactions, electron-neutral interactions and charged-charged interactions.

For air-aerosol mixtures, we considered 34 monatomic species (C, O, N, Si, Al, Fe, Ca, C^+, O^+, N^+, Si^+, Al^+, Fe^+, Ca^+, C^-, O^-, N^-, Si^-, Al^-, Fe^-, C^{++}, O^{++}, N^{++}, Si^{++}, Al^{++}, Fe^{++}, Ca^{++}, C^{+++}, O^{+++}, N^{+++}, Si^{+++}, Al^{+++}, Fe^{+++}, Ca^{+++}) and electrons; 31 diatomic species (C_2, O_2, N_2, Si_2, Al_2, Fe_2, Ca_2 CO, CN, SiC, AlC, NO, SiO, AlO, SiN, FeO, AlN, CaO, C_2^+, O_2^+, N_2^+, CO^+, CN^+, NO^+, AlO^+, CaO^+, N_2^-, C_2^-, O_2^-, CN^-, and AlO^-); and 40 polyatomic species (CO_2, C_3, CCN, CNC, CNN, C_2O, O_3, N_3, NCO, NO_2, N_2O, NCN, SiC_2, SiO_2, Si_2C, Si_2N, Si_3, AlC_2, AlO_2, Al_2O, OCCN, C_2N_2, CNCOCN, C_3O_2, C_4, NO_3, N_2O_3, N_2O_4, N_2O_5, Al_2C_2, Al_2O_2, Al_2O_3, $Fe(CO)_5$, N_2O^+, CO_2^+, Al_2O^+, $Al_2O_2^+$, AlO_2^-, NO_3^-, and NO_2^-).

For neutral-neutral interactions, we used collision integrals from Capitelli et al. [22] to consider the following interactions: O-C_2N, N-C_2, N-CN, N-CO, N-C_3, N-N_3, N-O_3, N-C_2N, N-CO_2, N-C_2O, N-NO_2, N-N_2O, N-CNO, NO-C_3, NO-N_3, NO-O_3, NO-C_2N, NO-CO_2, NO-C_2O, NO-NO_2, NO-CNO, NO_2-NO_2, N_2O-CNO, N_2O-N_2O, NO_2-CNO, NO_2-N_2O, N_2-CN, N_2-CO, N_2-NO, N_2-C_3, N_3-N_3, N_2-N_3, N_2-O_3, N_2-C_2N, N_2-C_2O, N_2-CO_2, N_2-NO2, N_2-N_2O, N2-CNO, N_3-O_3, N_3-C_2N, N_3-CO_2, N_3-C_2O, N_3-NO_2, N_3-N_2O, N_3-CNO, C-C_3, C-N_3, C-O_3, C-C_2N, C-CO_2, C-C_2O, C-NO_2, C-N_2O, C-CNO, C-N, C-O, C-C_2, C-N_2, C-O_2, C-CN, C-CO, CN-CN, CN-CO, CN-NO, CN-C_3, CN-N_3, CN-O_3, CN-C_2N, CN-CO_2, CN-C_2O, CN-NO_2, CN-N_2O, CN-CNO, CO-O_3, CO-C_2N, CO-CO_2, CO-C_2O, CO-NO_2, CO-N_2O, CO-CNO, CO-CO, CO-NO, CO-C_3, CO-N_3, CNO-CNO, C_2O-CNO, C_2-C_2, C_2-N_2, C_2-O_2, C_2-CN, C_2-CO, C_2-NO, C_2-C_3, C_2-N_3, C_2-O_3, C_2-C_2N, C_2-CO_2, C_2-C_2O, C_2-NO_2, C-C, C_2-N_2O, C_2-CNO, C_3-C_3, C_3-N_3, C_3-C_2N, C_3-CO_2, C_3-C_2O, C_3-NO_2, C_3-N_2O, C_3-CNO, C_3-O_3, C_2N-C_2N, C_2N-CO_2, C_2N-C_2O, C_2N-NO_2, C_2N-N_2O, C_2N-CNO, CO_2-CO_2, CO_2-C_2O, CO_2-NO_2, CO_2-N_2O, CO_2-CNO, C_2O-C_2O, C_2O-NO_2, C_2O-N_2O, O-CO_2, O-C_2O, O-NO_2, O-N_2O, O-CNO, O-C_2, O-CN, O-CO, O-NO, O-C_3, O-N_3, O-O_3, O_2-CN, O_2-CO, O_2-NO, O_2-C_3, O_2-N_3, O_2-O_3, O_2-C_3N, O_2-CO_3, O_2-C_2O, O_2-NO_2, O_2-CNO, O_2-N_2O, O_3-O_3, O_3-C_2N, O_3-CO_2, O_3-C_2O, O_3-NO_2, O_3-N_2O, and O_3-CNO [22]. Capitelli et al. give collision integrals for N_2-N_2, N_2-O_2, NO-NO, N-NO, N-N, N-N_2, N-O_2, NO-N_2, O-O, O-N_2, O-O_2, O_2-O_2, and N-O [29]. For the remaining neutral-neutral interactions, we used a Lennard-Jones 12-6 potential and its parameters (ε_{ij}, and σ_{ij}) according to the following equations

$$\begin{cases} \varepsilon_{ij} = \left(\varepsilon_i \varepsilon_j\right)^{1/2} \\ \sigma_{ij} = \frac{1}{2}\left(\sigma_i + \sigma_j\right) \end{cases} \quad (15)$$

$$\overline{\Omega}_{ij}^{(l,s)} = r_0^2 \left[\frac{A}{T^{*B}} + \frac{C}{\exp(DT^*)} + \frac{E}{\exp(FT^*)} + \frac{G}{\exp(HT^*)} + RT^{*B} \sin\left(ST^{*W} - P\right) \right] \quad (16)$$

where *A*, *B*, *C*, *D*, *F*, *G*, *H*, *S*, *P*, and *W* are defined by Neufeld [30]. Table 1 lists the Lennard-Jones parameters used to calculate the remaining collision integrals.

For the missing collision integrals, we used the approximation

$$\overline{\Omega}_{AB}^{(l,s)} = \sqrt{\Omega_A^{(l,s)^{1.5}} + \Omega_B^{(l,s)^{1.5}}} \quad (17)$$

For the neutral-charge interactions we used the collision integrals from the work of Capitelli et al. [29] for N −N^+, O−O^+, N −N^{++}, O−O^{++}, O−N^+, N −O^+, N_2-N_2^+, and O_2-O_2^+. For C−C^+, C−C^-, C−N^-, C-N^+, C-O^+, C-O^-, C-N_2^+, C-C_2^+, C-O_2^+, C-CN^+, C-CO^+, C-NO^+, C-CO_2^+, N-C^+, O-C^+, N_2-C^+, C_2-C^+, O_2-C^+, CN-C^+, CO-C^+, CO_2-C_2^+, N_2-C_2^+, O_2-C_2^+, CN-C_2^+, CO-C_2^+, NO−C^+, C_3−C^+, CO_2−C^+, N−C^-, O−C^-, C_2−C^-, N_2−C^-, O_2−C^-, CN−C^-, and CO−C^- collisions, they were obtained from the works of Capitelli et al. [22]. The other ion-neutral interactions were considered to be elastic collisions. The corresponding collision integrals were calculated using the theoretical expressions proposed by Kihara [37, 38].

$$\overline{\Omega}_{ij}^{(l,s)} = \left(\frac{Z_i^2 e^2 \xi}{2\pi\varepsilon_0 k_b T} \right)^{1/2} \left(\frac{\Gamma\left(s+\frac{3}{2}\right)}{\frac{(s+1)!}{2}} \frac{A_{(4)}^{(l)}}{\frac{2l+1-(-1)^l}{2(l+1)}} \right) \quad (18)$$

where $A_{(4)}^{(1)} = 0.6547$, $A_{(4)}^{(2)} = 0.3852$, and $A_{(4)}^{(3)} = 0.7166$, Z_i is the charge number of the charged particle, and ε_0 the permittivity of vacuum. The polarizability constants α used for the neutral particles are reported in Table 2. For load transfer, collisions have considerably larger cross-sections than elastic collisions. Charge transfer is equivalent to deflecting the particle from π-χ, where χ represents the angle of deviation in an elastic collision. The momentum transport cross-section is then written as:

$$Q_{tr}^{(n)} = 2\pi \left[\int_0^\infty (1-P_{ex})\left(1-\cos^n\chi\right)\sin\chi d\chi + \int_0^\infty P_{ex}\left(1-\cos^n(\pi-\chi)\right)\sin\chi d\chi \right] \quad (19)$$

where P_{ex} is the probability of charge exchange, and n is the index of the n^{th} potential curve. If n is even, the terms that contain them P_{ex} disappear, the collision becomes elastic, and the charge is exchanged. The effective odd-order collision integrals are considered to be the result of the geometrical mean of the elastic and inelastic resonant contributions:

$$\Omega^{(l,s)} = \sqrt{\Omega_{el}^{(l,s)^2} + \Omega_{ex}^{(l,s)^2}} \quad (20)$$

For electron neutral interactions, collision integrals of *e*−O, *e*−C, *e*−N, *e*−N_2, *e*−O_2, *e*−CO, and *e*−NO were obtained from Capitelli et al. [22]. For *e*−Si, *e*−Si_2, *e*−SiO_2, and *e*−SiO collisions we used data from Andr é et al. [33] while Andr é et al. [26] was used for *e*−C_3, *e*−CO_2, *e*−C_2, *e*-O_3, and *e*−CN. The last collision integrals for *e*-Al, *e*-Fe, *e*-Al_2, *e*-Fe_2, *e*-AlN, *e*-AlO, *e*-FeO, *e*-CaO, *e*-CNN, *e*-C_2O, *e*-N_3, *e*-NO_2, *e*-N_2O, *e*-NCN, *e*-AlO_2, *e*-Al_2O, *e*-C_2N_2, *e*-C_3O_2, *e*-C_4, *e*-NO_3, *e*-N_2O_3, *e*-N_2O_4, *e*-N_2O_5, *e*-Al_2O_2, *e*-Ca, *e*-CaO, *e*-AlC, *e*-SiC, *e*-Ca_2, *e*−SiC_2, *e*-Si_2C, *e*-Si_2N, *e*-Si_3, *e*-AlC_2, *e*-OCCN, *e*-CNCOCN, *e*-Al_2O_3, *e*-SiN, *e*−$Fe(CO)_5$, and *e*-AlN interactions were obtained using the polarisability method (Equation 18).

Interactions between charged species were described by the screened Coulomb potential using the Debye radius as the screening distance. We used the collision integrals established by Devoto [41] from the momentum transport cross-sections given by Liboff [40], written as:

$$\begin{cases} \overline{\Omega}_{ij}^{(1,s)} = \left[\frac{4}{s(s+1)}\right] b_0^2 \left[\ln(\Lambda) - \frac{1}{2} - 2\bar{\gamma} + \Psi(s)\right] \\ \overline{\Omega}_{ij}^{(2,s)} = \left[\frac{12}{s(s+1)}\right] b_0^2 \left[\ln(\Lambda) - 1 - 2\bar{\gamma} + \Psi(s)\right] \end{cases} \quad (21)$$

where

$$\begin{cases} b_0 = \frac{Z_i Z_j e^2}{2k_b T} \\ \Lambda = \frac{2\lambda_D}{b_0} \\ \Psi(s) = \sum_{n=1}^{s-1} \frac{1}{n} \\ \Psi(1) = 0 \\ \bar{\gamma} = 0.5772 \\ \lambda_D = \left(\frac{k_b T}{4\pi n_1 e^2}\right)^{1/2} \end{cases}$$

In this study, only electrons were considered for computing the Debye length according to Mason's work [42].

Table 1. *(12, 6) Lennard-Jones parameters used in our calculation.*

Species	σ_{ij} (Å)	ε_{ij} (K)	References	Species	σ_{ij} (Å)	ε_{ij} (K)	References
C	3	100	[26]	NCO	3.828	232.4	[31]
CO	3.60	100	[26]	NO_2	3.765	210	[35]
CO_2	4	200	[26]	N_2O	3.828	232.4	[35]
CNC	3.828	252	[31]	NCN	3.577	71.850	[32]
C_2	3.621	97.53	[26]	NO_3	3.462	114.810	[35]
CNN	3.557	71.850	[32]	N_2O_3	3.381	198.06	[35]
C_2O	3.487	57.867	[32]	N_2O_4	4.621	347	[35]
C_3	3.649	48.33	[32]	N_2O_5	3.276	197.086	[35]
C_3O_2	3.538	79.757	[32]	N	2.98	119	[26]
C_2N_2	4.661	349	[31]	N_2	3.68	91.5	[26]
Si	3.3	3170	[33]	N_2-N	3.33	104.5	[26]
FeO	4.7604	565.774	[34]	N_2 -O_2	3.557	101.85	[26]
Fe	4.3	3000	[28]	N2-NO	3.6	109.14	[26]
Fe_2	5.417	3000	[28]	NO	3.53	105	[26]
Al	2.655	2570	[28]	O	2.8	117	[26, 33]
Al_2	2.940	2570	[28]	O_2	3.499	100	[26]
AlN	3.369	443.439	[35]	O_2-O	3.011	107.3	[26]
AlO	3.204	541.687	[35]	O_2-NO	3.479	111.65	[26]
AlO_2	3.044	557.449	[35]	O-NO	3.150	120.5	[26]
Al_2O	2.995	541.689	[35]	O_3	3.756	100	[26]
Al_2O_2	3.186	557.449	[35]	Ca	3.60	2497	[36]
N_3	3.199	75.918	[35]				

Table 2. *Polarisability constants of neutral species used in the calculation code.*

Species	Value (10^{-30}.m^3)	Reference	Species	Value (10^{-30}.m^3)	Reference
Fe	8.40	[28]	Al_2O_2	18.261	[35]
Fe_2	16.80	[28]	*Si*	5.38	[33]
FeO	9202	[34]	Si_2	10.76	[33]
CNN	3.96	[32]	SiO	6.18	[33]
C	1.76	[26]	SiO_2	6.98	[33]
NCN	3.96	[32]	O_2	1.6	[32]
C_3O_3	6.884	[32]	O	0.802	[26]
CO	1.95	[26, 32]	O_3	3.21	[32]
C_2N_2	7.99	[32]	N_3	2.7	[32, 35]
C_3	4.9	[26, 32]	N_2	1.753	[32]
C_2O	3.2	[32]	*N*	1.10	[26]

Species	Value ($10^{-30}.m^3$)	Reference	Species	Value ($10^{-30}.m^3$)	Reference
C_4	7.04	[32]	*NO*	1.70	[26, 32]
CO_2	2.911	[24]	NO_2	3.02	[32]
CN	2.1	[32]	N_2O	3.03	[34, 35]
Al	8.34	[28]	NO_3	3.506	[35]
Al_2	16.68	[28]	N_2O_3	4.606	[35]
AlN	9.44	[35]	N_2O_4	6.69	[35]
AlO	9.142	[35]	N_2O_5	6.210	[35]
AlO_2	9.921	[35]	Ca	22.8	[nist]
Al_2O	17.482	[35]	CaO	2.841	[39]

Table 3. *Comparative analysis of the transport properties.*

Temperature	Electrical conductivity ($\Omega^{-1}m^{-1}$)			Thermal conductivity ($W.m^{-1}K^{-1}$)			Dynamical Viscosity ($kgm^{-1}s^{-1}$)		
	Capitelli	Result	Differences (%)	Capitelli	Result	Differences (%)	Capitelli	Result	Differences (%)
7000	327.7	317.36	3.26	4.27	4.41	3.85	2.33E-4	2.15E-4	8.37
10000	3264	2997.51	8.89	1.37	1.45	5.51	2.61E-4	2.58E-4	1.16
15000	8418	7562.64	11.3	3.66	3.30	10.9	8.61E-5	8.21E-5	4.87
	Boulos	Result	Differences (%)	Pascal	Result	Differences (%)	Pascal	Result	Differences (%)
7000	264.1	317.36	16.78	3.71	4.41	15.87	2.04E-4	2.15E-4	5.11
10000	2705.5	2997.51	9.64	1.44	1.45	0.7	2.41E-4	2.58E-4	5.59
15000	7796.4	7562.64	3.09	3.43	3.30	1.30	7.62E-5	8.21E-5	7.18

3. Results

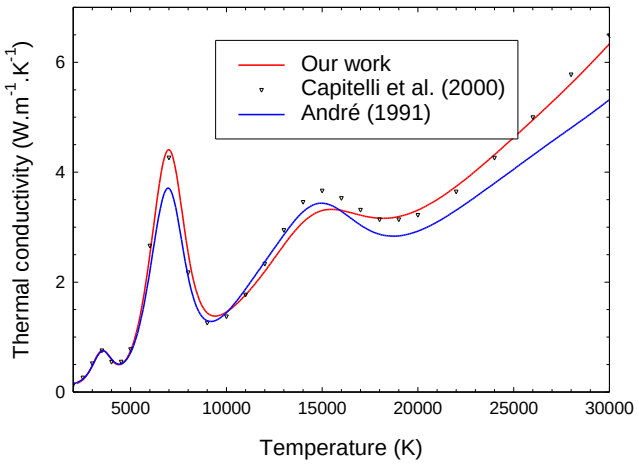

Figure 3. *Thermal conductivity of air plasma at atmospheric pressure. Comparison with the literature.*

The transport properties of air-aerosol mixtures under the assumption of the LTE were evaluated for a temperature range of 2,000 to 30,000 K, and atmospheric pressure. These properties depend on the plasma composition, as previously described.

There were no existing data were available for the air-aerosols mixtures proposed in this work. However, previous research has focused on other pure gases or mixtures, including air, nitrogen, carbon dioxide (CO_2), CF_3I, argon - copper, argon - aluminium, C_4F_7N-CO_2-O_2, air-PA_{66}-copper, or C_4F_7N plasmas [43-54] for example.

To validate our code MATLAB, we compared our results with those already published data such as those of dry air plasma [43-46].

The transport properties are listed in Table 3. Figures 3-5 compare thermal conductivity, electrical conductivity, and dynamic viscosity with data from Boulos et al. [43], Pascal [55], and Capitelli et al. [22]. Our results being Capitelli et al [22]. Our electrical conductivity at 7,000 K differs by 16.78% with Boulos et al. [43] and 3.26% with Capitelli et al. [22], while 15.87% and 3.85% are observed between our thermal

conductivity and data given by Pascal [55] and [22] respectively. Better agreement is obtained by comparison with those of Capitelli because we used the same collision integrals for neutral-neutral, neutral-charged and electron-neutral interactions. The differences with other works may be due to the choice of interaction potentials (Hulbert-Hirschfelder or Lennard-Jones potentials), as well as the methods used to obtain collision integrals (numerical or approximation methods). Furthermore, the expression used to calculate the Debye length: considering both electrons and ions or electrons only, significantly impacts the charge-charge interactions and therefore the results at high temperatures (T>20,000 K). We did not choose the same interaction potentials as those authors in our code, due to the lack of details in their studies.

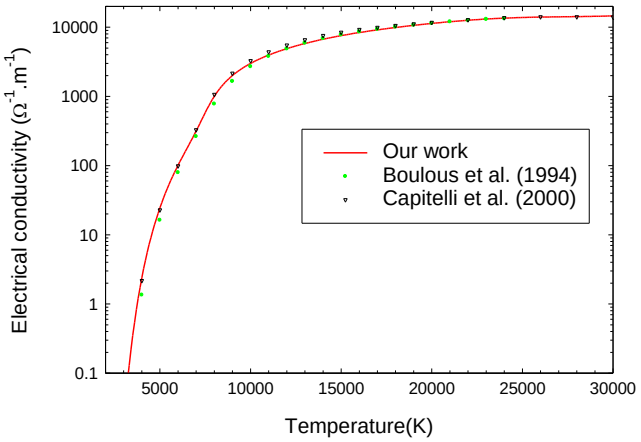

Figure 4. *Electrical conductivity of the air plasma at atmospheric pressure. Comparison with the literature.*

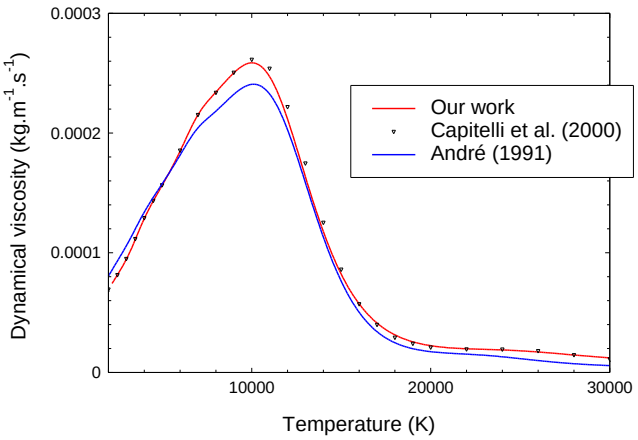

Figure 5. *Viscosity of air plasma at atmospheric pressure. Comparison with the literature.*

at ~3,500 K, a second peak at ~7,000 K for all curves, and a third peak at ~15,000 K. These peaks are caused by dissociation and ionisation reactions. The first peak is attributed to the dissociation of CO_2, FeO, AlC, CN, SiC, AlC, SiN, NO, O_2, Al_2O, SiO_3 and, other polyatomic molecules. The second peak is attributed to the dissociation of N_2 and CO. The third peak is related to the ionisation of C, O, and N. The influence of ions Al^+, Fe^+, Ca^+ and Si^+ resulting from the mixture appears for temperatures between 13,000 K and 20,000 K. In this temperature range, conductivity is closely related to diffusion-type collision integrals (l=1). For temperatures above 20,000 K, the thermal conductivity is mainly due to the translation of electrons, with plasmas almost totally ionized. The thermal conductivity strongly depends on the reaction thermal conductivity at temperatures corresponding to the dissociation and ionisation temperatures of the various particles.

Thermal conductivity is a very important property since it characterises the ability of a plasma to evacuate the heat stored by the creation of the arc and is therefore directly linked to the arc lifetime. Therefore, this property gives information about the interruption capability of a gas. Its importance is particularly evident in its reaction component, following equation [56]:

$$\tau.\lambda_R^{\max} = C^t \tag{22}$$

with, C^t is a constant, τ the arc lifetime and $\lambda_R^{\max}$ the maximum of the reaction thermal conductivity. Thus, the higher the maximum reaction thermal conductivity, the shorter the arc lifetime.

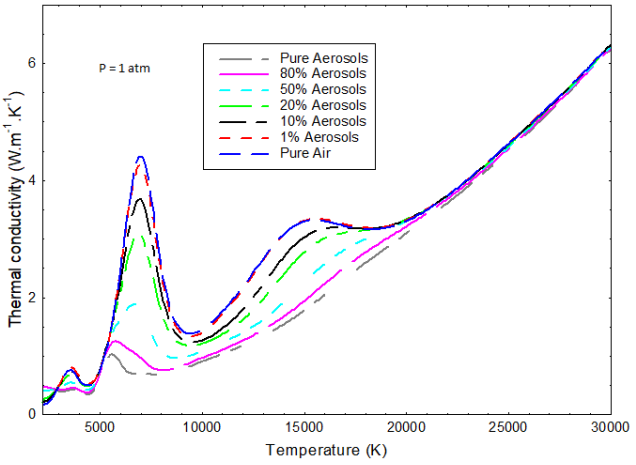

Figure 6. *Thermal conductivity of air-aerosol mixtures at atmospheric pressure.*

4. Discussion

The total thermal conductivities of the various mixtures plotted in Figure 6 show the same behaviour, with a first peak

In Figure 6, we can observe that air plasma has the highest thermal conductivity and that the presence of dust in the mixture decreases the thermal conductivity, except at temperatures below 3,000 K. These lower values are due to the

low dissociation and ionisation energies of the aerosol particles. The reaction thermal conductivity of air at 7,000 K is equal to 3.81 $W.m^{-1}K^{-1}$, an addition of 1% aerosol reduces it to 3.67 $W.m^{-1}K^{-1}$, while 10% addition reduces it to 3.02 $W.m^{-1}K^{-1}$. This decrease can lead to an extension of the arc lifetime, which is detrimental to the arc cut-off and to the rapid dielectric regeneration in the arc chamber. Aerosols can therefore cause circuit breaker failure.

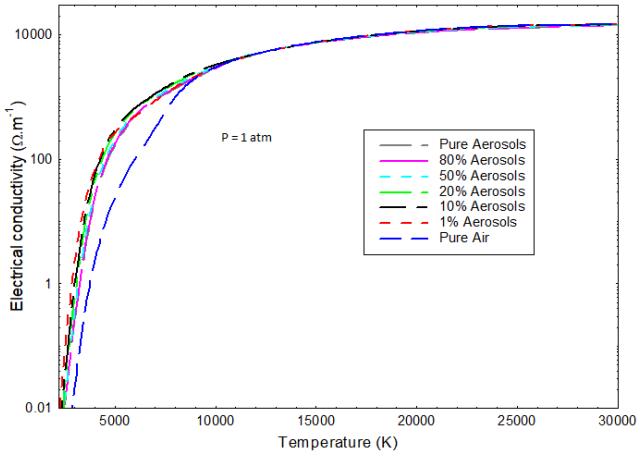

Figure 7. *Electrical conductivity of air-aerosol mixtures at atmospheric pressure.*

Figure 7 shows the evolution of electrical conductivity as a function of temperature and aerosol proportion. This coefficient varies very rapidly with temperature. Very low electrical conductivity values are observed for low temperatures and high values for high temperatures (e.g., the electrical conductivity of a mixture of 99% air - 1% aerosols is equal to 70.16 $\Omega^{-1}m^{-1}$ at 4,000 K and 3,037.37 $\Omega^{-1}m^{-1}$ at 10,000 K). At low temperatures (<10,000 K), electron-neutral collisions strongly affect the behaviour of this property because they vary proportionally to the square of the number density of electron populations which varies rapidly due to the ionisation phenomena. Indeed, this density increases considerably when the mixture contains species having weak ionisation energies (this is the case for metallic or alkaline species). Therefore, a very small concentration of aerosols in the mixture tends to increase both the electron population and the electrical conductivity at low temperatures (<10,000 K). At 4,000 K, the electrical conductivity of pure air is equal to 2.39 $\Omega^{-1}m^{-1}$ while that of a mixture of 99% air-1% aerosols is equal to 70.16 $\Omega^{-1}m^{-1}$ (an increase of more than 2900%). However, and for temperatures below 6,000 K, if more than 10% aerosols are added to the mixtures, the electrical conductivity tends to decrease compared to the values of the mixture with 10%. This decrease can be explained by the increase in oxygen, carbon and silicon in the medium which leads to higher concentrations of negative ions and molecules like C_2, O_2, CO_2, C_3, NO, SiO at low temperatures. The consequences are that this presence of aerosols increases the capacity of the plasma to conduct the current which could delay the cut-off of the electric arc and the dielectric regeneration in the arc chamber. For temperatures above 10,000 K, the values are almost similar regardless of the mixtures. Collisions between charged particles gradually became the main interactions, and the density of the electron population number density remains almost constant with increasing temperature. The increase in electron density is balanced by the increase in the collision cross-section, which can be attributed to a greater degree of ionisation. For these temperatures, the electrical conductivity therefore exhibits the same behaviour and no longer varies according to the nature of the plasma because the plasma is almost completely ionised.

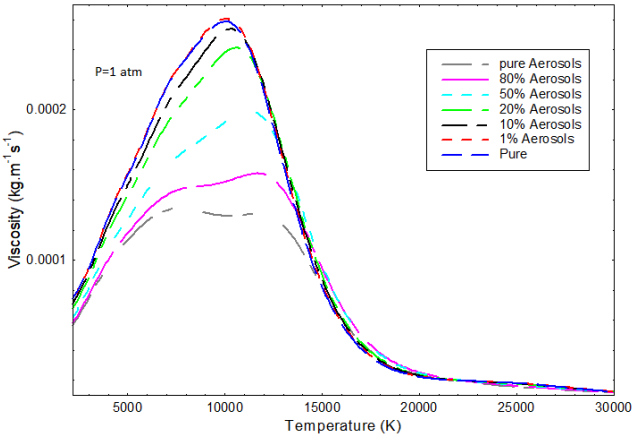

Figure 8. *Viscosity of air-aerosols mixtures at atmospheric pressure.*

Figure 8 shows the results obtained for the viscosities of pure air and air-aerosol mixtures. We observe similar shapes, with a coefficient that varies according to the square root of the product of the temperature and mass and that is inversely proportional to ($\overline{\Omega}_{ij}^{(2,2)}$) which strongly impacts the behaviour of the dynamical viscosity. The maximum viscosity is reached between 10,000 K and 11,000 K. The amplitude and position of this peak depend on the ionisation energies and mass of the species. Indeed, this peak marks the transition between plasmas first governed by neutral particles (and collisions between neutral particles) and then by charges particles (atomic ions and electrons). The decrease of the coefficient at medium and high temperatures is explained by a higher binary diffusion and a dominance of Coulomb interactions resulting from the various ionisations. Concerning the influence of the nature of the plasma, the dynamic viscosities of air-aerosol are lower than those of pure air at low temperatures. This phenomenon is explained by the lower ionisation potentials of the c aerosol constituents (silicon, carbon, aluminium, and iron) compared to those of oxygen and nitrogen. These low values lead to a rapid increase in electrons in the medium, counterbalanced by an increase in charged particles, thus leading to a faster transition to an

ionised plasma, and therefore to an earlier appearance of the peak. The higher the proportion of aerosols in the medium, the lower the viscosity of the plasma, for temperatures below 13,000 K. These variations are all the more significant because aerosol the concentration is high.

When the current is cut off in a circuit breaker, the arc extinction relies on the mechanisms responsible for cooling the medium and/or the re-ignition in it. Thus, a high viscosity helps to slow down charged particles and reduces their diffusion. Arc energy is dissipated more efficiently by combining viscosity effects with convection (gas blowing) or radiation phenomena. During the breaking phase, aerosols could induce the circuit breaker malfunctions.

5. Conclusions

In this work, we investigated the effect of aerosols on the transport coefficients of an air plasma in a local thermodynamic equilibrium. The results showed that an increase in the proportion of aerosols in the mixture led to a complete modification of the interrupting medium. The maximum dynamic viscosity was reached between 10,000 K and 11,000 K, and decreased as the aerosol concentration increased, with all plasmas showing a rapid decrease above 13,000 K. Finally, electrical conductivity increased with the proportion of aerosols or oxides in the mixture, thermal conductivity showed peaks at approximately 3,500 K, 7,000 K, and 15,000 K and generally decreased with more aerosols, except when temperatures are below 3,000 K.

This theoretical analysis demonstrated that aerosols had a significant impact on plasma characteristics, including electrical conductivity, thermal conductivity, and dynamic viscosity.

A good interrupting medium must have high thermal and low electrical conductivities at low temperatures, and rapid dielectric recovery. In addition, the plasma must be a good electrical insulator at low temperatures to facilitate transient recovery voltage and avoid restrikes. The results showed that the presence of aerosols reduced the thermal conductivity. This would increase the lifetime of the arc. Thus, being detrimental to the cooling efficiency of the plasma gas in a circuit breaker. They also showed that they increased electrical conductivity, potentially promoting leakage currents, and that they can lead to oxide and carbon deposits in the interrupting chamber.

While transport coefficients are not sufficient to determine the interrupting capacity of a circuit breaker, they provide information on the impact of aerosols on this capacity. Thus, this present work should be supplemented by studies of dielectric strength properties, density variations, energy fluxes and radiation effects, by conducting experiments to comprehensively characterise plasma properties, including the influence of solid-phase aerosols.

Abbreviations

LTE Local Thermodynamic Equilibrium

Author Contributions

Yaguibou Wepari Charles: Conceptualization, Data curation, Formal Analysis, Investigation, Methodology, Resources, Writing – original draft, Writing – review & editing

Pafadnam Ibrahim: Formal Analysis, Investigation, Methodology, Project administration, Resources, Software, Supervision, Validation, Writing – review & editing

Banouga Adjigkiga: Methodology, Software, Supervision, Validation, Visualization, Writing – review & editing

Yann Cressault: Resources, Software, Supervision, Validation, Visualization, Writing – original draft, Writing – review & editing

Kagone Abdoul Karim: Project administration, Resources, Software, Supervision, Validation, Visualization, Writing – review & editing

Kohio Niessan: Resources, Software, Supervision, Validation, Visualization, Writing – original draft, Writing – review & editing

Koalaga Zacharie: Resources, Software, Supervision, Validation, Visualization, Writing – original draft, Writing – review & editing

Data Availability Statement

The data is available from the corresponding author upon reasonable request.

The data supporting the outcome of this research work has been reported in these manuscripts:

Capitelli M, Bruno D, and Larichiuta A 2013 Fundamental Aspects of Plasma Chemical Physics Transport (New York: Springer Series on Atomic, Optical, and Plasma Physics 74) p 364.

Boulos I M, Fauchais P, and Pfender E 1994 Thermal Plasmas: The Fundamentals and Applications (New York: Plenum Press) 413-417.

D'angola A, Colonna G, Gorse C and Capitelli M 2008 Eur. Phys. J. D 46 129-150.

Conflicts of Interest

The authors declare no conflicts of interest.

References

[1] Louvert S Modulations intra saisonnières de la mousson d'Afrique de l'Ouest et impacts sur les vecteurs du paludisme à Ndiop (Sénégal): diagnostics et prévisibilité. *PhD Thesis* Université de Bourgogne (France) 2008.

[2] Legrand M Étude des aérosols sahariens au-dessus de l'Afrique à l'aide du canal à 10 microns de METEOSAT: Visualisation, interprétation et modélisation. *PhD Thesis* Université des Sciences et Techniques de Lille Flandres Artois (France) 1990.

[3] Malavelle F Effets direct et semi-direct des aérosols en Afrique de l'Ouest pendant la saison sèche. *PhD Thesis* Université Toulouse III Paul Sabatier (France) 2011.

[4] Pancrati O. Analyse et modélisation des impacts des aérosols sahéliens sur le cycle hydrologique en Afrique de l'Ouest: Rôle des poussières et de la biomasse brûlée, *PhD Thesis* Université des Sciences et Technologies de Lille (France) 2003.

[5] Bruno K. Caractérisation optique et microphysique des aérosols atmosphériques en zone urbaine ouest africaine: application aux calculs du forçage radiatif à Ouagadougou, PhD Thesis Université de Ouagadougou, Ouagadougou (Burkina Faso) 2014.

[6] Bouh H A, Benyaich F, Bounakhla M, Noack Y, Tahri M and Zahry F. Variations Saisonnières des particules atmosphériques et ses composants chimiques dans la Ville de Meknès - Maroc (Seasonal variations of the atmospheric particles and its chemical components in Meknes city-Morocco). Journal: Journal of Materials and Environmental Science 2013. 4 (1) 49-62.

[7] Antenne G J Y. Le phénomène des brumes sèches au Sénégal. Bulletin n7 de l'Office de la Recherche Scientifique et Technique d'Outre-Mer (ORSTOM) et du Centre de Météorologie Spatiale (Sénégal) 1985.

[8] Tobias C and Megie. Les lithométéores au Tchad: Premiers résultats concernant la nature, la composition et l'importance des aérosols transportés par voie atmosphérique dans la région de N'Djamena (Tchad). l'Office de la Recherche Scientifique et Technique d'Outre-Mer (*O.R.S.T.O.M)*, 1980-1981 *vol* 18(1) 71-82.

[9] Herrmann L, Bleich K E, Sterk, Stahr K. Dépôt des poussières sur les sols en Afrique de l'Ouest: Propriétés et source des poussières et influence sur les propriétés des sols et sites. Year Université de Hohenheim, Institut pour la Science du sol et Ecologie (310) 1997.

[10] Orange D and Gac J Y. Geochemical Assessment of Atmospheric Deposition Including Harmattan Dust in Continental West Africa, *Proc. IAHS* 1993.

[11] Orange D and Gac J Y. Bilan géochimique des apports atmosphériques en domaines sahélienne et sou-dano-guinéen d'Afrique de l'ouest (bassins supérieurs du Sénégal et de la Gambie), *Géodynamique* 1990, 5 51-65.

[12] Doumbia E H T. Caractérisation physico-chimique de la pollution atmosphérique en Afrique de l'Ouest et étude d'impact sur la santé, *PhD Thesis* Université Toulouse III - Paul Sabatier (France) 2012.

[13] Michaud V. Modélisation et diagnostic de plasmas thermiques utilisés pour la coupure de l'arc électrique, *PhD Thesis* Université Blaise Pascal de Clermont-Ferrand (France) 2009.

[14] Flament P, Deboudt K, Cachier H, Châtenet B and Mériaux X. Mineral Dust and Carbonaceous Aerosols in West Africa: Source Assessment and Characterization. *Atmospheric Environment, 2011 45, 3742-3749.* https://doi.org/10.1016/j.atmosenv.2011.04.013

[15] Hadji T D E 2012 *PhD Thesis* Université de Toulouse III (France).

[16] André P, Courty M A, Kagoné A K, Koalaga Z K, Kohio N K and Zougmoré F. Calcul de la composition chimique dans un plasma issu de mélanges de PTFE, d'air, de cuivre et de vapeur d'eau dans le cadre d'appareillages de coupure électrique à air, Journal International de Technologie, de l'Innovation, de la Physique, de l'Énergie et de l'Environnement. 2016, 2(1) 1.

[17] Yaguibou W C, Kohio N, Kagoné A K, Koalaga Z and Zougmoré F. Influence des aerosols sur la composition à l'équilibre d'un plasma d'air. Journal International de Technologie, de l'Innovation, de la Physique, de l'Énergie et de l'Environnement 2018. 4(1) 1.

[18] Koalaga Z. Contribution à l'étude expérimentale et théorique des plasmas d'arc laminés, *PhD Thesis* Université de Clermont Ferrand II (France) 1991.

[19] Devoto R S. Simplified Expressions for the Transport Properties of Ionized Monatomic Gases. *Physics of Fluids.* 1967, 10 2105. https://doi.org/10.1063/1.1762005

[20] Muckenfuss C and Curtiss C. F. Thermal Conductivity of Multicomponent Gas Mixtures. *Journal Chemical of Physics.* 1958, 29(6) 1273-1277. https://doi.org/10.1063/1.1744709

[21] Capitelli M 1977 Transport properties of partially ionized gases. *Journal de Physique. Colloq.* 38(C3) 227.

[22] Capitelli M, Bruno D, and Larichiuta A. Fundamental Aspects of Plasma Chemical Physics Transport (New York: Springer Series on Atomic, Optical, and Plasma Physics. 2013, 74 p 364.

[23] Kagoné A K, Koalaga Z and Zougmoré F. Calculation of air-water vapor mixtures thermal plasmas transport coefficients. *IOP Conf. Series: Materials Science and Engineering.* 2012 *Conf. Ser.* 29 1. https://doi.org/10.1088/1757-899X/29/1/012004

[24] Butler N J and Brokaw S R. Excitation Function for the Reaction T(d,n)He^4. Physical Review. 1957, 106, 1636. https://doi.org/10.1103/PhysRev.106.272

[25] Brokaw R S. Viscosity and thermal conductivity of high-temperature reacting gas mixtures. The Journal of Chemical Physics. 1960. 32, 1005. https://doi.org/10.1063/1.1730896

[26] André P, Brunet L, Bussiere W, Caillard J, Lombard J M and Picard J P. Transport coefficients of plasmas consisting of insulator vapours. European Physical Journal - Applied Physics. 2004, 25 169-182. https://doi.org/10.1051/epjap:2004007

[27] Yaguibou W C, Kohio N, Kagone A K and Koalaga Z. Impact of Aerosol on Transport Coefficients of Air Thermal Plasmas in Circuit Breakers. International Journal of Engineering Research. 2018, 7(4) 43-47. https://doi.org/10.5958/2319-6890.2018.00094.6

[28] Cressault Y, Murphy A. B, Teulet Ph, Gleizes A and Schnick M. Thermal plasma properties for Ar-Cu, Ar-Fe and Ar-Al mixtures used in welding plasmas processes: II. Transport coefficients at atmospheric pressure. Journal of Physics D: Applied Physics. 2013, 46(41). https://doi.org/10.1088/0022-3727/46/41/415207

[29] Capitelli M, Gorse C and Longo S. Collision Integrals of High-Temperature Air Species. Journal of Thermophysics and Heat Transfer. 2000, 14:2, pp. 259-268

[30] Neufeld P D, Janzen A R and Aziz R. Empirical Equations to Calculate 16 of the Transport Collision Integrals $\Omega^{(l, s)^*}$ for the Lennard - Jones (12-6) Potential. The Journal of Chimical Physics. 1972, 57 1100-1102. https://doi.org/10.1063/1.1678363

[31] Amadou S and Baronnet J M. Transport Coefficients of Ar/C/H/O/N Systems Thermal Plasma at Atmospheric Pressure. IOP Conference Series: Materials Science and Engineering 2012, 29 012003 1-27.

[32] Cressault Y, Connord V, Hingana H, Teulet Ph and Gleizes A. Transport properties of CF_3I thermal plasmas mixed with CO2, air or N_2 as an alternative to SF_6 plasmas in high-voltage circuit breakers. Journal of Physics D: Applied Physics 2011, 44 495202. https://doi.org/10.1088/0022-3727/44/49/495202

[33] Andr é P, Bussiere W and Rochette D. Transport Coefficients of Ag-SiO2 Plasmas. Plasma Chemistry and Plasma Processing. 2007, 27, 381-403. https://doi.org/10.1007/s11090-007-9086-y

[34] Cressault Y, Hannachi R, Teulet P, Gleizes A, Gonnet J P and Battandier J Y. Influence of metallic vapours on the properties of air thermal plasmas. Plasma Sources Science and Technology 2008, 17, 035016. https://doi.org/10.1088/0963-0252/17/3/035016

[35] Cressault Y, Gleizes A and Riquel G. Properties of air-aluminum thermal plasmas. Journal of Physics D: Applied Physics 2012, 45, 265202 (12pp). https://doi.org/10.1088/0022-3727/45/26/265202

[36] Khoei A R, Aramoon A, Jahanbakhshi F, DorMohammadi H. A coupling atomistic-continuum approach for modelling mechanical behavior of nano-crystalline structures. Computational Mechanics January 2014, 1-18.

[37] Taro K et Marion H. T, and Joseph O. H. Transport Properties for Gases Assuming Inverse Power Intermolecular Potentials. The Physics of Fluids, 1960, 3 (5) 715-720 http://dx.doi.org/10.1063/1.1706115

[38] Gorse C and Capitelli M 2001 Atomic and Plasma-Material Interaction Data for Fusion (APID series vol 9) ed (USA) D R S (Wagramer Strasse 5, P. O. Box 100, A-1400 Vienna, Austria: International Atomic Energy Agency).

[39] Gussoni M, Rui M and Zerbi G. Electronic and relaxation contribution to linear molecular polarizability. An analysis of the experimental values Journal of Molecular Structure. 1998, 447, 163-215.

[40] Liboff R L. Transport Coefficients Determined Using the Shielded Coulomb Potential. The Physics of Fluids. 1959, 2(1) 40-46, http://dx.doi.org/10.1063/1.1724389

[41] Devoto R S. Transport Coefficients of Partially Ionized Argon. The Physics of Fluids. 1967 10(2) 354-364, http://dx.doi.org/10.1063/1.1762115

[42] Mason E A, Munn R. J and Francis J. S. Transport Coefficients of Ionized Gases. The Physics of Fluids. 1967, 10(8) 1827-1832.

[43] Boulos I M, Fauchais P, and Pfender E 1994 Thermal Plasmas: The Fundamentals and Applications (New York: Plenum Press) 413-417.

[44] D'angola A, Colonna G, Gorse C and Capitelli M. Thermodynamic and transport properties in equilibrium air plasmas in a wide pressure and temperature range. The European Physical Journal D. 2008, 46, 129-150, https://doi.org/ 10.1140/epjd/e2007-00305-4

[45] Colonna G, D'Angola A, Laricchiuta A, Bruno D and Capitelli M. Analytical Expressions of Thermodynamic and Transport Properties of the Martian Atmosphere in a Wide Temperature and Pressure Range. Plasma Chem. Plasma Process. 2013, 33, 401-431.

[46] Capitelli M, Colonna G, Gorse C and A. D'Angola. Transport properties of high temperature air in local thermodynamic equilibrium. The European Physical Journal D. 2000, 11 279-289.

[47] Cressault Y and Gleizes A. Thermal plasma properties for Ar-Al, Ar-Fe and Ar-Cu mixtures used in welding plasmas processes: I. Net emission coefficients at atmospheric pressure. Journal of Physics D: Applied Physics. 2013, 46, 415206 (16pp). https://doi.org/10.1088/0022-3727/46/41/415206

[48] Tanaka Y, Yokomizu Y, Kato M, Matsumura T, Shimizu K, Takayama S and Okada T. Electrical and Thermal Conductivities and Enthalpy of Air Plasma Contaminated with Fe, Ca, Mg or H_2O Vapour. 4th International Thermal Plasma Processes Conference (Athens, Greece, 15-17 July). 1996, p 587. https://doi.org/10.1615/ITPPC-1996.690

[49] Yokomizu Y, Ochiai R and Matsumura T. Electrical and thermal conductivities of high-temperature CO_2-CF_3I mixture and transient conductance of residual arc during its extinction process. Journal of Physics D: Applied Physics. 2009, 42(21), https://doi.org/10.1088/0022-3727/42/21/215204

[50] Colombo V, Ghedini E and Sanibondi P. Thermodynamic and transport properties in non-equilibrium argon, oxygen and nitrogen thermal plasmas. Progress in Nuclear Energy. 2008, 50 (8), 921-933. https://doi.org/10.1016/j.pnucene.2008.06.002

[51] Chervy B, Gleizes A and Razafinimanana M. Thermodynamic properties and transport coefficients in SF_6-Cu mixtures at temperatures of 300-30000 K and pressures of 0.1-1 MPa. Journal of Physics D: Applied Physics. 1994, 27, 1193. https://doi.org/10.1088/0022-3727/27/6/017

[52] Junwei D, Boya Z, Minchuan C, Guanyu W, Shizhe C, Zhoujing W, Xingwen L and Anthony B. M. Radiation properties of [C4F7N-CO2-O2]-PTFE-Cu mixtures at high temperatures and pressures for high-voltage circuit breakers. Journal of Physics D: Applied Physics. 2025, 58, 015206 (11pp) https://doi.org/10.1088/1361-6463/ad809d 2024

[53] Cressault Y, Kimpeler S, Moser A and Teulet Ph. Thermophysical properties of air-pa66-copper plasmas for Low-voltage direct current switches. Plasma Physics and Technology. 2023, 10 (1), 52-55. https://doi.org/10.14311/ppt.2023.1.52

[54] Zhong L, Wang J, Xu J, Wang X and Rong M. Effects of Buffer Gases on Plasma Properties and Arc Decaying Characteristics of C_4F_7N-N_2 and C_4F_7N-CO_2 Arc Plasmas. lasma Chemistry and Plasma Processing. 2019, 39, 1379-96.

[55] André P. Etude de la composition et des propriétés thermodynamiques des plasmas thermiques à l'équilibre et hors d'équilibre thermodynamique. PhD Thesis Université Blaise Pascal de Clermont-Ferrand II (France). 1995.

[56] Koalaga Z, Abbaoui M and Lefort A. Calcul des propriétés thermodynamiques des plasma d'isolants $C_\alpha H_\beta O_\gamma N_\theta$. Journal of Physics D: Applied Physics. 1993, 26 393-403.

Biography

Yaguibou Wepari Charles is a teacher at Thomas SANKARA University, Dori University Cente. He completed his PhD in Plasma Physics and Electric Arcs from Joseph KI-ZERBO University in 2018, and his Master of Applied Physics from the same institution in 2014. Dr. Yaguibou was promoted to the rank of Maître-Assistant (Assistant Professor) by CAMES in 2023.

Banouga Adjigkiga earned his Master's degree in 2018 and recently defended his Ph.D. in 2024 at Joseph KI-ZERBO University. His research, conducted at the Laboratory of Materials and Environment, focused on plasma physics. His thesis work specifically investigated the impact of a silver-tin dioxide alloy ($AgSnO_2$) on the transport and thermodynamic properties of plasmas in circuit breakers. In addition to his research career, Mr. Banouga also works as a high school teacher.

Pafadnam Ibrahim is an assistant at the Science and Technology Training and Research Unit at Thomas SANKARA University in Ouagadougou. He obtained his PhD in applied physics in 2024 from Joseph KI-ZERBO University in Ouagadougou. He has participated in numerous international research projects in recent years. He has also participated in several international conferences on various topics. Dr. Ibrahim PAFADNAM is passionate about scientific research and innovation.

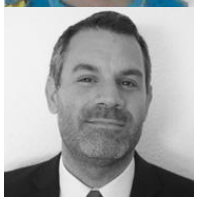

Yann Cressault was born, in France. He received the Ph.D. degree in physics and plasma discharge engineering from Paul Sabatier University, Toulouse, France, in 2001. He spent four years in Theoretical Physics with Orsay University, Orsay, France, from 1993 to 1997, and one year in Plasmas Physics in 1998 with Paul Sabatier University. From 2002 to 2004, he was a Temporary Teacher and a Researcher with Blaise Pascal University, Clermont-Ferrand, France. Since 2004, he has been a Lecturer with Paul Sabatier University and develops his research with the LAPLACE Laboratory, Toulouse, France. His teaching activities are mainly focused on plasmas, electrotechnics, and electronics. More specifically, he develops both theoretical and experimental research on radiative transfer and on the transport properties of thermal plasmas in local thermodynamic equilibrium and in nonequilibrium state. His current research interests include the optimization of thermal plasmas processes with the presence of electric arcs (circuit breakers, plasma torches, plasma welding, plasma cutting, and arc furnace). Dr. Cressault is a member of the French Association Arc Electrique and the French network Plasmas Froids.

Kohio Niessan is a teacher-researcher at the Ecole Normale Supérieure in Burkina Faso. He defended his PhD on February 12, 2016 at Joseph KI-ZERBO University. He is a specialist in electric arc plasmas, where he has published around twenty scientific articles in indexed international journals. He has also been an external CAMES evaluator since 2021.

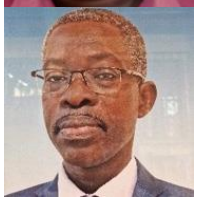

Koalaga Zacharie holds a Ph.D. in Electrotechnics from Université Blaise Pascal, France, earned in 1991. He is a distinguished Full Professor in Electronic, Electrotechnics, and Photovoltaic at the UFR-SEA Department of Physics. Currently, he serves as the Director of the Laboratory of Materials and Environment (LAME) at UJKZ, a position he has held since 2020. is extensive career includes significant leadership roles, such as serving as the President of the Scientific Council for both the ESUP-Jeunesse School and the IFIC-AUF in Tunis. He has also directed the open and distance learning institute at UJKZ and was the Academic Director of the ISGE-BF Institute. is research expertise lies in the physics of electrical arcs and plasmas, as well as photovoltaic systems. A prolific academic, he has supervised 14 Ph.D. theses and over 50 Master's dissertations. He actively coordinates research projects and conferences, including the RAMSES Network Center of Excellence and the ISAPA Symposium 2011. Additionally, he is a scientific editor for the *Journal International de Technologie, de l'Innovation, de la Physique, de l'Energie et de l'Environnement* (JITIPEE) and a member of several professional organizations, including the IEEE.

Research Field

Yaguibou Wepari Charles: Plasma Physics, Electric Arcs, Waste Management, Environment, Energy
Pafadnam Ibrahim: Plasmas, Electric Arcs, Environment, Energy, Climat
Banouga Adjigkiga: Plasmas, Electric Arcs
Kagone Abdoul Karim: Plasma Physics, Electric Arcs, Waste Management, Environment, Energy
Kohio Niessan: Plasma Physics, Electric Arcs, Waste Management, Environment, Energy
Yann Cressault: radiative transfer, transport properties of thermal plasmas in local thermodynamic equilibrium and in nonequilibrium state and optimization of thermal plasmas processes
Koalaga Zacharie: Electrical arc and Plasmas Physics, Photovoltaic systems